Optics Letters

Aberration-free pupil steerable Maxwellian display for augmented reality with cholesteric liquid crystal holographic lenses

Jianghao Xiong,[1] ^{iD} Yannanqi Li,[1] Kun Li,[2] and Shin-Tson Wu[1],[*] ^{iD}

[1]*College of Optics and Photonics, University of Central Florida, Orlando, Florida 32816, USA*
[2]*GoerTek Electronics, 5451 Great America Parkway, Suite 301, Santa Clara, California 95054, USA*
Corresponding author: swu@creol.ucf.edu

Maxwellian displays offer unique features like always-in-focus quality, high efficiency, and large field-of-view, but its small eyebox remains a major challenge for augmented reality. To enlarge the eyebox, pupil steering is a promising approach. However, previous pupil steering methods generally rely on changing the incident light angle on the lens coupler, which results in serious aberrations. In this Letter, we demonstrate a pupil steerable see-through Maxwellian display incorporating novel cholesteric liquid crystal (CLC) holographic lenses. By actively modulating the polarization state of the incident light, we can schematically choose which holographic lens to function, which fundamentally eliminates the aberrations. © 2021 Optical Society of America

Augmented reality (AR) refers to blending digital information into the real world. It is a promising next generation display for ubiquitous digital interaction. This objective, however, brings several technical challenges, such as form factor, field-of-view (FOV), image brightness, and vergence-accommodation conflict (VAC) [1–3]. All these issues need to be tackled simultaneously in a display system while keeping the see-through capability.

For a specific display system, several trade-off relations exist among the above-mentioned parameters. For example, in an AR display adopting traditional optics like half-mirror and refractive surfaces, the conservation of étendue leads to a trade-off between the FOV and eyebox [1]. A larger étendue would result in a larger form factor. In a waveguide display [2,3], the conservation of étendue is broken due to multiple outcouplings in the total internal reflection (TIR) process, so that the eyebox can be increased without compromising the FOV. However, a large eyebox implies that most of the light does not enter the viewer's eye, which leads to a compromised image brightness. To enable an AR display for outdoor applications, high image brightness is critical to prevent the washout problem, especially when the ambient light is strong [3]. Additionally, the FOV of a waveguide display is constrained by the TIR process and is limited to ∼60° [4].

Maxwellian displays [5–16], as another promising approach, have attracted increasing interest lately. In a Maxwellian display, the collimated imaging light is focused on a spot called the viewpoint. When the viewpoint is located at the viewer's pupil, the image can be directly formed on the retina, as Fig. 1 depicts. To build a Maxwellian display, different configurations can be used, including system with a collimated light source and a spatial light modulator (SLM) [5–11], or a laser scanning system with vibrating micro-mirrors [12–15].

A unique feature of the Maxwellian display is that the image is always in focus no matter which depth the viewer is watching. This deprivation of the viewer's focus cue can partially solve the VAC, which is a major problem in near-eye displays [17]. Another advantage of the Maxwellian display is that its FOV is theoretically unlimited, as long as the lens coupler in Fig. 1 can accommodate a small enough f-number. Furthermore, the Maxwellian display also exhibits a very high overall optical efficiency, because nearly all the light is delivered into the viewer's eye if the lens coupler has a reasonably high efficiency.

However, the major drawback of the Maxwellian display is its tiny eyebox. In this sense, Maxwellian displays can be regarded as an extreme case to trade the eyebox for the FOV. Because the size of each viewpoint should be much smaller than the pupil diameter, the eyebox size is equal to that of the pupil diameter, which typically ranges from about 2 mm to 4 mm in a bright environment [18]. To enlarge the eyebox, several approaches
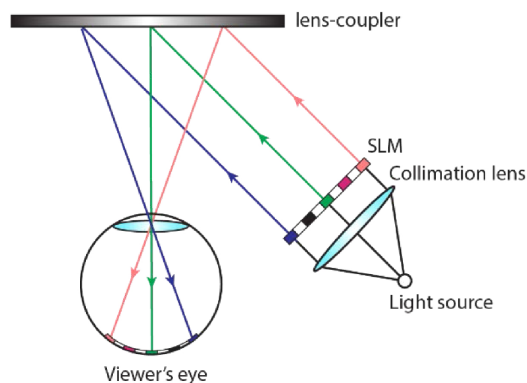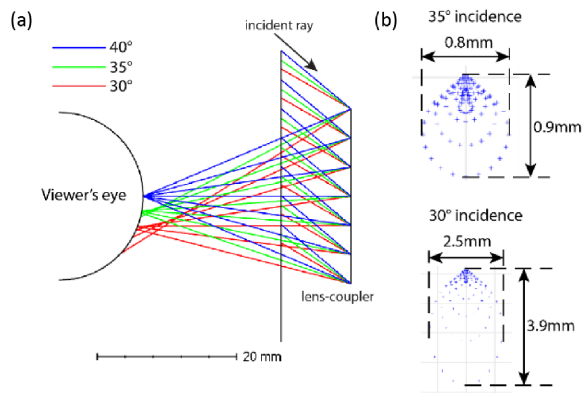

Fig. 1. Schematic view of a Maxwellian display.

Fig. 2. Raytracing model of pupil steering by changing the incident angle: (a) $\theta = 40°$, $35°$, and $30°$. (b) Spot diagrams at $\theta = 35°$ and $30°$.

Fig. 3. LC director configuration and polarization response of a CLC holographic grating.

have been proposed, which can be categorized into pupil duplication [8,12,15] and pupil steering [5,7,10,13,14,19]. Pupil duplication uses a multiplexed hologram [8] or duplicating incident rays [12,15] to form multiple viewpoints. Although it expands the eyebox, the efficiency decreases accordingly. Besides, if the separation of viewpoints is smaller than the pupil size, more than one Maxwellian view would enter the viewer's eye, causing ghost images [8,15]. This issue becomes more complicated because the pupil diameter of the human eye varies dynamically as the ambient light brightness changes.

Therefore, pupil steering is deemed to be a better solution without the concerns of decreased efficiency and ghost imaging although it requires an additional eye tracking module to determine the steering position. Almost all previous pupil steering methods rely on changing the incident light angle through beam steering techniques like SLM [5,10], backlight modulation [7], or a scanning mirror [13]. These methods, however, introduce a severe aberration because the lens coupler can only have diffraction-limited performance at one incident angle. Meanwhile, the inclusion of an additional beam steering module increases the system complexity and volume.

In this Letter, we demonstrate a new pupil steering approach with a novel cholesteric liquid crystal holographic lens (CLCHL) and a switchable polarization converter. Instead of relying on changing the incident angle to shift the focal point, our proposed system uses a polarization converter to manipulate the light polarization and select a proper holographic lens to function. Since the incident angle is fixed, aberrations can be eliminated completely because each CLCHL can be diffraction-limited.

To evaluate the influence of the incident angle on aberrations, we simulate an off-axis diffractive lens coupler, as shown in Fig. 2(a). The lens coupler is assumed to be diffraction-limited at incident angle $\theta = 40°$. Its diameter is 24 mm, and the focal length is 30 mm. The diameter of the viewer's eye is 24 mm. When θ changes from $40°$ to $35°$ and then to $30°$, the focal spot shifts by 2.1 mm and 4.4 mm, respectively. But the spot diagram shown in Fig. 2(b) indicates that the spot size increases to 0.8 mm by 0.9 mm at $\theta = 35°$ and 2.9 mm by 3.9 mm at $\theta = 30°$. Note that the spot size at $\theta = 30°$ is almost equal to the pupil size. This would result in a distorted image at the retina, compromised always-in-focus quality, and decreased FOV.

A traditional diffractive lens coupler is made of holographic photopolymers, where the intensity of the interfering field
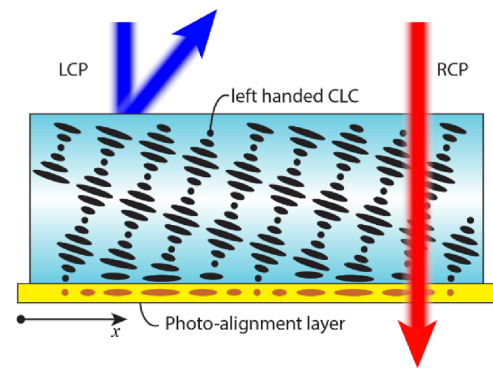
pattern is recorded as refractive index modulation [20]. This type of holographic element usually exhibits a small angular and spectral bandwidth due to its small index modulation. Its response to light is also polarization insensitive. Recently, a new diffractive optical element fabricated by photo-alignment polarization holography (PAPH) is developed, which has found widespread applications [21,22]. When a CLC is used in PAPH, a tilted helical structure is formed [23], as shown in Fig. 3. The bottom alignment determines the pattern period in the x direction, which governs the diffraction angle. The bulk helical structure, say left-handed, establishes a strong Bragg reflection for the left-handed circularly polarized (LCP) light. For the right-handed circularly polarized (RCP) light, its diffraction efficiency is nearly zero. This strong polarization selectivity offers a new modulation method using an active polarization converter to control the incident polarization.

The working principle of our proposed system is illustrated in Fig. 4. The lens coupler module consists of two switchable half-wave plates (HWPs) and two CLCHLs (L1 and L2). The function of the HWP is to convert the incident LCP light to RCP at a voltage-on state, while retaining its original polarization state at the voltage-off state, while L1 and L2 are designed to work under LCP light. When HWP1 is at off state, the incident LCP light maintains the polarization state after HWP1 and gets coupled by L1 into viewpoint A, as Fig. 4(a) shows. When HWP1 and HWP2 are both at on-state, the incident LCP is first converted to RCP after HWP1, and then it passes through L1 due to the polarization selectivity. Afterward, it is converted back to LCP state after HWP2 and gets coupled by L2 into viewpoint B. Note that the incident angle is fixed in the whole process. If L1 and L2 are recorded in the same configuration, aberrations can be eliminated completely by choosing a diffraction-limited template lens. Finally, it is worth mentioning that more viewpoints can be achieved by stacking additional pairs of CLCHL and the polarization converter accordingly. By controlling the polarization converters, we can choose the desired CLCHL to function and steer the light to the designated viewpoint.

To build a proof-of-concept demo, we fabricated two CLCHLs with opposite handedness. This way, only one HWP is required to steer the pupil. We used a blue laser ($\lambda = 457$ nm) in the interferometer for photo-alignment exposure. A collimated reference beam was incident at $45°$ to the substrate. A template aspheric lens with a focal length of 35 mm was placed in the recording beam. The relative angle of the recording beam to the
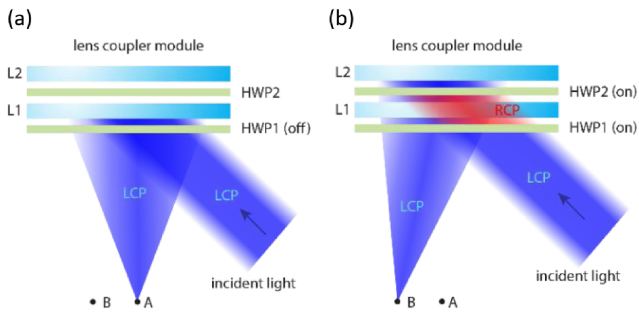
(a)   (b)

Fig. 4. Working principle of the proposed system. Incident light is steered into (a) viewpoint A and (b) viewpoint B.

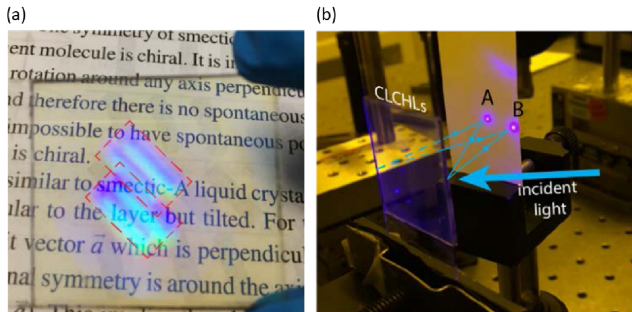(a)   (b)

Fig. 5. Fabricated CLCHLs. (a) Photo of the fabricated lenses with two images of the ceiling lamp formed by each lens individually, as indicated by the red dashed boxes. (b) Photo of the focusing behavior of the CLC HLs with an oblique incident light and formation of two focal points A and B.

substrate is 90° for viewpoint A and 77° for viewpoint B, so that the two viewpoints have an 8 mm spatial separation. To fabricate a CLCHL, a thin layer of photo-alignment material (brilliant yellow) was spin-coated on a cleaned glass substrate. Then the sample was placed in the interferometer for exposure with a dosage of 0.7 W/cm². Then a liquid crystal reactive mesogen RM257 doped with chiral R/S5011 was spin-coated on the exposed substrate, forming the holographic lens pattern. The sample was polymerized under UV curing. The detailed fabrication process has been reported in [4]. Two fabricated CLCHLs were laminated together using an optical glue NOA67.

Figure 5(a) shows a photo of the fabricated CLCHLs. The text behind the lenses is clearly readable, indicating a good see-through capability. The images of ceiling lamps (red boxes) are formed by two CLCHLs accordingly. Figure 5(b) shows the focusing performance of the CLC lenses. The incident light is a collimated 457 nm laser light, whose incident angle is 45°. Two viewpoints A and B are formed, with a measured spot size of around 50 µm. The deviation from diffraction-limited performance results from the small misalignment in experiment. The efficiencies of both lenses are measured to be about 60%, which can be adjusted by controlling the sample thickness.

The switchable HWP can be fabricated using a homogeneous alignment, vertical alignment, or twisted nematic (TN) LC cell combined with a quarter-wave plate. In our experiment, we used a homogeneous cell filled with a 2-µm-thick LC material DIC LC-1 ($\Delta n = 0.284$, $\Delta \varepsilon = 7.53$). To verify its property as a polarization converter, we used an input RCP light ($S3 = 1$) at 45° incident angle and measured the S3 parameter of the output light with different applied voltages. Results are shown
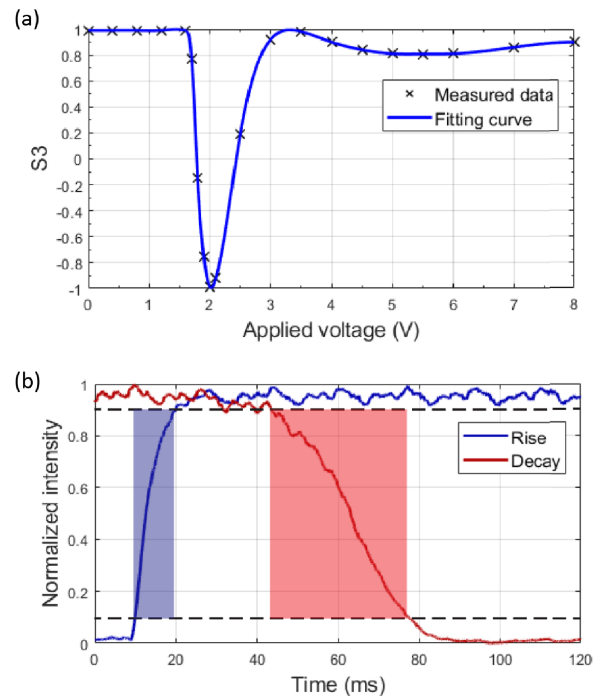
(a)

(b)

Fig. 6. (a) Measured voltage-S3 curve of our fabricated polarization converter. (b) Measured rise time and decay time of our fabricated polarization converter between 0 and 2 V.

in Fig. 6(a). The output S3 is close to 1, corresponding to phase retardation $\delta = 2\pi$, when the voltage is below the threshold. As the voltage increases to 2 V, S3 changes to −1, indicating LCP state and $\delta = \pi$. Therefore, we can use 0 V and 2 V as the off- and on-state for the polarization converter. The switching time between 0 and 2 V is shown in Fig. 6(b). The rise time is about 10 ms, and decay time is about 33 ms, giving a total response time of 43 ms. The response time can be improved by choosing a lower viscosity LC material [24] and optimizing the cell structure. It is worth mentioning that if the incident light is broadband instead of a laser, then the TN polarization rotator is preferred [25].

With the fabricated CLCHLs and switchable polarization converter, we demonstrated a pupil steerable Maxwellian display with a laser projector (SONY MP-CL1). The blue laser in the projector has a wavelength $\lambda = 445$ nm, which is close to our recording laser wavelength (457 nm). The configuration of our system is shown in Fig. 7.

The light from the laser projector first passes through a neutral density (ND) filter (1/16) and is collimated by a lens ($f = 30$ mm). The collimated light is then incident on the polarization converter and then the CLCHLs. The reason we included a ND filter was to lower the image brightness so that we could obtain a high contrast photo. To simulate a human pupil, we used a smartphone camera with about a 2 mm pupil diameter to capture the images.

The photos of the real scene and displayed image are shown in Figs. 8(a) and 8(b). The captured images at two viewpoints are shown in Figs. 8(c) and 8(d). We can see that even after the ND filter the image is still quite bright, which indicates a high ambient contrast ratio (ACR). Display devices with such a high ACR can well accommodate the daily usage even in a bright outdoor environment, which is considered a challenging task for
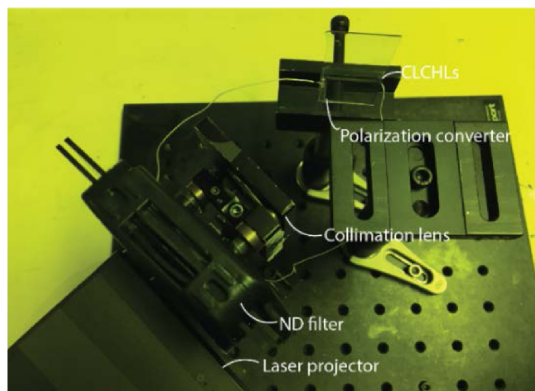
Fig. 7. Photo of our optical system. The beams from the laser projector are dimmed and collimated before reaching the polarization converter and CLCHLs.
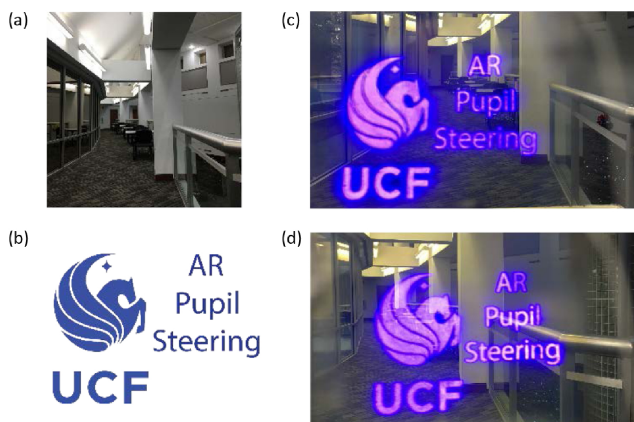

Fig. 8. (a) Photo of the scene without the display system. (b) Displayed picture. Captured images of our AR display system for (c) viewpoint A and (d) viewpoint B.

other AR architectures like waveguide displays. The see-through scene appears a little yellowish due to the blue light diffraction from CLCHLs. This issue can be alleviated by using CLCHLs with a lower efficiency. The image resolution is determined by the laser projector. The used portion has a resolution of around 500 by 500. With a system FOV of around 44°, the resolution density is about 18 pixels per degree.

Finally, let us discuss the potential compactness of our system for more viewpoints and full-color displays. The thickness of both the CLCHL and switchable LC layer is only several microns, while the thickness of the coupler module is determined by the glass substrates. In the most compact form, adding another CLCHL and polarization converter requires an additional glass substrate, with both LC material and CLCHL film in between. Recently, an ultra-thin glass (30 μm) substrate has been developed for flexible displays. For a conservative estimate, if each glass substrate is 0.1-mm-thick, then the total thickness of 10 viewpoints is 1 mm, which is still quite compact. Of course, more layers would result in a dimmed background, which can be alleviated by adopting CLCHLs with a lower

efficiency. Full-color image can also be achieved by integrating CLCHLs working in red–green–blue wavelengths. Although the recording of CLCHLs uses a blue laser, the aberrations for red and green colors can still be eliminated if we design a freeform template lens to pre-compensate for the related aberrations from wavelength mismatch.

In conclusion, we demonstrate a pupil steerable Maxwellian AR display system. Such a system utilizes the polarization dependent property of CLCHLs as a coupler and includes polarization converters to dynamically control which coupler to function. Our approach eliminates the optical aberrations and simplifies the system design. Widespread applications for near-eye displays and advanced imaging systems are foreseeable.

Disclosures. The authors declare no conflicts of interest.

Data Availability. Data underlying the results presented in this paper are not publicly available at this time but may be obtained from the authors upon reasonable request.

REFERENCES

1. O. Cakmakci and J. Rolland, J. Disp. Technol. **2**, 199 (2006).
2. B. C. Kress, *Optical Architectures for Augmented-, Virtual-, and Mixed-Reality Headsets* (SPIE, 2020).
3. Y.-H. Lee, T. Zhan, and S.-T. Wu, Virtual Reality Intell. Hardware **1**, 10 (2019).
4. J. Xiong, G. Tan, T. Zhan, and S.-T. Wu, OSA Continuum **3**, 2730 (2020).
5. C. Chang, W. Cui, J. Park, and L. Gao, Sci. Rep. **9**, 18749 (2019).
6. H. Do, Y. M. Kim, and S.-W. Min, Appl. Opt. **58**, 2882 (2019).
7. M. K. Hedili, B. Soner, E. Ulusoy, and H. Urey, Opt. Express **27**, 12572 (2019).
8. S.-B. Kim and J.-H. Park, Opt. Lett. **43**, 767 (2018).
9. J. S. Lee, Y. K. Kim, and Y. H. Won, Opt. Express **26**, 19341 (2018).
10. J.-H. Park and S.-B. Kim, Opt. Express **26**, 27076 (2018).
11. Y. Takaki and N. Fujimoto, Opt. Express **26**, 22985 (2018).
12. C. Jang, K. Bang, G. Li, and B. Lee, ACM Trans. Graph. **37**, 195 (2018).
13. C. Jang, K. Bang, S. Moon, J. Kim, S. Lee, and B. Lee, ACM Trans. Graph. **36**, 190 (2017).
14. J. Kim, Y. Jeong, M. Stengel, K. Akşit, R. Albert, B. Boudaoud, T. Greer, J. Kim, W. Lopes, Z. Majercik, P. Shirley, J. Spjut, M. McGuire, and D. Luebke, ACM Trans. Graph. **38**, 99 (2019).
15. T. Lin, T. Zhan, J. Zou, F. Fan, and S.-T. Wu, Opt. Express **28**, 38616 (2020).
16. G. Westheimer, Vis. Res. **6**, 669 (1966).
17. G. Kramida, IEEE Trans. Vis. Comput. Graph. **22**, 1912 (2016).
18. A. B. Watson and J. I. Yellott, J. Vis. **12**(10), 12 (2012).
19. A. R. L. Travis, L. Chen, A. Georgiou, J. Chu, and J. Kollin, J. Soc. Inf. Disp. **26**, 526 (2018).
20. J. Xiong, K. Yin, K. Li, and S.-T. Wu, Adv. Photon. Res. **2**, 2000049 (2021).
21. Q. Chen, Z. Peng, Y. Li, S. Liu, P. Zhou, J. Gu, J. Lu, L. Yao, M. Wang, and Y. Su, Opt. Express **27**, 12039 (2019).
22. S. Lee, M. Wang, G. Li, L. Lu, Y. Sulai, C. Jang, and B. Silverstein, Sci. Rep. **10**, 16127 (2020).
23. J. Xiong, R. Chen, and S.-T. Wu, Opt. Express **27**, 18102 (2019).
24. H. Chen, F. Gou, and S.-T. Wu, Opt. Mater. Express **7**, 195 (2017).
25. Y.-H. Lee, G. Tan, T. Zhan, Y. Weng, G. Liu, F. Gou, F. Peng, N. V. Tabiryan, S. Gauza, and S.-T. Wu, Opt. Data Process. Storage **3**, 79 (2017).